To appear in *The Astrophysical Journal (Letters)*

The Evolution of the Distribution of Star Formation Rates in Galaxies

Lennox L. Cowie,[1,2] Esther M. Hu,[1,2] Antoinette Songaila[1]
Institute for Astronomy, University of Hawaii, 2680 Woodlawn Dr., Honolulu, HI 96822
cowie@ifa.hawaii.edu, hu@ifa.hawaii.edu, acowie@ifa.hawaii.edu

and

Eiichi Egami[2]
Max-Planck-Institut für extraterrestrische Physik, 85740 Garching, GERMANY
egami@mpe-garching.mpg.de

ABSTRACT

A large deep and nearly complete $B < 24.5$ redshift sample is used to measure the change in distribution function of the stellar mass production rate in individual galaxies with redshift. The evolution of the star formation rate distribution with redshift is interpreted in terms of the history of spiral galaxy formation, with the disk component modelled as a single evolving entity, and the characteristic timescales, luminosities, and epochs varying according to galaxy type. The more massive forming galaxies seen at $z = 1 \rightarrow 3$ are identified as earlier type spirals, whose star formation rates are initially high and then decline rapidly at $z < 1$, while for later type spirals and smaller mass irregulars the mass formation rates at $z < 1$ are lower, and the formation process persists to redshifts much closer to the present epoch. We find that these models can be consistent with the data and fit well into a broad picture of other recent results if q_0=0.02 and many of the disks begin their growth at $z \ll 3$, but that they predict too many bright star formers at high z in flat universes.

Subject headings: cosmology: observations — galaxies: evolution — galaxies: formation — galaxies: fundamental parameters — surveys

---

[1]Visiting Astronomer, W. M. Keck Observatory, jointly operated by the California Institute of Technology and the University of California.

[2]Visiting Astronomer, United Kingdom Infrared Telescope, operated by the Joint Astronomy Centre on behalf of the U. K. Particle Physics and Astronomy Research Council.

1. Introduction

Disks of spiral galaxies are extremely fragile and must have formed primarily by conversion of gas to stars in an essentially invariant galaxy potential with only a small accretion of external stars (e.g., Toth & Ostriker 1992). Thus, the stellar history of this component may be approximately modelled as the evolution of a single entity, which greatly simplifies predicting the luminosity evolution. In the present Letter we trace the evolution of the distribution of star formation rates in galaxies with redshift to determine whether it is consistent with this type of pure luminosity evolution. The problem is relatively straightforward because beyond $z \sim 0.3$ the observed B band corresponds to ultraviolet light ($\lambda \ll 3500\,\text{Å}$), which in all but the oldest galaxies is a measure of the ongoing rate of massive star formation. The B luminosity is then directly proportional to the rate of metal production in the individual galaxy, while the contribution of the ensemble of galaxies to the extragalactic background light measures the overall metal density production in the universe (Cowie 1988; Songaila, Cowie, & Lilly 1990; Lilly et al. 1996; Madau et al. 1996). Viewed this way, deep B-band redshift samples measure the distribution function of the stellar mass production rate in galaxies, which we will refer to as the $\dot{M}$ function, in contrast to infrared samples, which for all but the youngest galaxies measure the distribution of the mass in galaxies.

In order to probe star formation rates (SFR) in individual galaxies to high redshifts, large and extremely deep B-band redshift samples are required. Here we use a large, 95% complete sample of galaxies to $B = 24.5$ with redshifts to $z = 2.2$, to measure the evolution of the $\dot{M}$ function with redshift. We find that smooth single-entity evolution models can work if q_0=0.02 and many disks begin to form only at later epochs, but predict too many bright star formers at high z in flat universes.

2. Data

Cowie et al. (1996) described LRIS observations of a $B = 24.5$ galaxy sample in the Hawaii fields SSA13 and SSA22 (26.2 arcmin^2). However, even the more intensively studied SSA22 field was only 84% complete at $B = 24-24.5$, with 13 $B \leq 24.5$ galaxies unidentified. Since extremely high completeness is required to determine the $\dot{M}$ function and the unidentified objects may correspond to higher redshift objects in the sample, we made intensive efforts to complete identifications of the remaining $B \leq 24.5$ galaxies in SSA22 using deeper optical (3500–10000 Å) observations and near infrared spectroscopy. The improved S/N and additional spectral features yield robust identifications for all but four sample objects.

The SSA22 $B < 24.5$ sample is used with a nearly complete $B < 24$ sample in SSA13. In the $B < 24$ sample covering 26 arcmin^2 there are 156 objects (124 galaxies) of which all but 4 are identified (97% complete), while in the $B = 24 - 24.5$ range covering 13 arcmin^2 there are 47 objects (42 galaxies) of which all but 2 are identified (95% complete). The six unidentified galaxies have extremely blue colors but no strong [O II], with most likely redshifts $1.6 < z < 2$, where the [O II] line has moved from the observed optical while many stronger UV features have not yet entered the blue wavelength range. However, some objects may lie at somewhat higher redshifts.

The redshift-magnitude relation and median redshifts are shown in Figure 1, along with the Autofib sample of Ellis et al. (1996). As at brighter magnitudes, the median B redshifts, computed from the combination of the Autofib data plus the present sample, are well described by a model (solid line) in which the luminosity function remains invariant (Broadhurst, Ellis, & Shanks 1988; Colless et al. 1990; Cowie, Songaila, & Hu 1991; Glazebrook et al. 1995a; Cowie et al. 1996), though this reflects a much more complex underlying situation. Dashed and dotted lines show expected magnitudes for a flat F_ν galaxy with $M_{AB} = -19.8 + 5 \log h_{65}$ for q_0=0.5 (dashed) and $M_{AB} = -20.5 + 5 \log h_{65}$ for q_0=0.02 (dotted), which roughly map the upper envelope of the magnitude-redshift relation at $1 < z < 2$. As we shall see below these correspond to star formation rates of roughly $9\, h_{65}^{-2}$ M$_\odot$ yr^{-1} (q_0=0.5) and $16\, h_{65}^{-2}$ M$_\odot$ yr^{-1} (q_0=0.02). As Cowie et al. (1996) emphasized, there are few galaxies with such high star formation rates at $z \ll 1$, and the envelope of the observed distribution lies well to the right of the curves at these redshifts, except for a few luminous AGN present in the samples. The brighter $z = 2 - 3$ galaxies lie to the left of the line, with mass formation rates up to a factor of 2.5 higher. (The Autofib and HDF data are not used in the remainder of the paper in order to avoid completeness problems.)

3. Interpretation

The present $B < 24.5$ sample provides two independent measurements of the massive star formation rate. The first is the rest-frame far UV ($\lambda \ll 3500$ Å) light, which for galaxies with significant ongoing star formation is a direct measure of the massive star formation rate, and hence of the metal production rate (Cowie 1988; Songaila et al. 1990). Translating this to a total star formation rate requires an uncertain assumption about the slope of the IMF. For a Salpeter IMF extending over the range $0.1 \rightarrow 125$ M$_\odot$ we may calibrate from the Bruzual & Charlot (1996) models to obtain, in the absence of internal extinction,

$$\dot{M} = 100 \ \mathrm{M}_\odot \, \mathrm{yr}^{-1} \left(\frac{L\,(2500\,\text{Å})}{6.7 \times 10^{29} \ \mathrm{ergs \ s^{-1} \ Hz^{-1}}} \right) \ , \qquad (1)$$

where a rest-frame wavelength of 2500 Å is chosen to minimize extrapolations from the B band in lower redshift galaxies while also minimizing the slight contamination by older stars which is present at slightly longer wavelengths. Equation (1) may be derived from extremely simple physical arguments and is quite model independent except for the assumed IMF (Cowie 1988). 2500 Å corresponds to B at $z = 0.8$ and I at $z = 2.4$, and may be interpolated at intermediate redshifts using approximate galaxy types inferred from the (B, I, K) galaxy colors, so that the 2500 Å luminosity can be relatively accurately determined at least at the higher redshifts. The massive star formation rate can also be obtained from the line luminosities in the galaxies, which measure the production rate of ionizing photons. The most direct diagnostic is $L(\mathrm{H}\alpha)$, which can be measured in these galaxies from $z = 0 \rightarrow 2.3$. For most of the galaxies, however, Hα is not measured, and we must draw on the secondary indicator [O II] 3727 Å, whose equivalent width is closely related to that of Hα by the relationship $\mathrm{W}_\lambda(\mathrm{H}\alpha{+}[\mathrm{N\,II}]) = 2.3\ \mathrm{W}_\lambda([\mathrm{O\,II}])$ in a wide variety of local and moderate redshift galaxies (Kennicutt 1992; Songaila et al. 1994). For local blue irregular galaxies (Gallagher, Bushouse, & Hunter 1989)

$$\dot{M} = 100\ \ \mathrm{M}_\odot\,\mathrm{yr}^{-1} \left(\frac{L\,([\mathrm{O\,II}])}{10^{43}\ \mathrm{ergs\ s}^{-1}} \right)\ , \tag{2}$$

but we derive an essentially identical calibration for the present galaxies by comparison with the more direct UV luminosity calibration, suggesting that this calibration is reasonable for most rapidly star-forming galaxies irrespective of mass and redshift. The [O II] luminosity provides an independent check on the UV luminosity which is particularly valuable at the low redshift end (Cowie, Hu, & Songaila 1995).

Internal extinction in the galaxies is a serious concern for both diagnostics, since escaping UV photons can be reduced significantly by this effect, while the internal production of Hα and [O II] can be reduced if ionizing photons are extinguished. However, at least for the higher redshift blue galaxies there appears to be remarkably little extinction and this effect appears weak. The great bulk of the $z > 0.8$ galaxies are extremely flat in the rest-frame 2500 Å−21000 Å color, with a median value of 0.9 in the AB system, and have high rest-frame [O II] equivalent widths (with a median of 40 Å). Since the intrinsic spectrum is expected to be flat or falling with increasing frequency, this places very severe constraints on the amount of dust. For a Seaton (1979) law $A_{2500} \approx\ E(2500\,\text{Å} - 10000\,\text{Å}) \approx\ 7\,E(B-V)$. Even if F_ν is intrinsically flat, $A_{2500} = 0.9$ on average, and at most half the light is lost to extinction. Thus, the maximum uncertainty introduced by not including an extinction correction is probably a factor of 2. To allow for the extinction we therefore assume that the luminosities in equations (1) and (2) are reduced by a factor of 1.5 for a given mass formation rate.

The computed rest-frame 2500 Å and [O II] luminosities are shown versus redshift in Figure 2. For q_0=0.02 and $H_0 = 65$ km sec^{-1} Mpc^{-1} (Fig. 2a) the upper envelope of the 2500 Å luminosity at $z > 1$ lies at approximately $10^{29}\ h_{65}^{-2}$ ergs s^{-1} Hz^{-1} and just above $10^{42}\ h_{65}^{-2}$ ergs s^{-1} for [O II], which correspond to mass formation rates in the $15 - 30\ h_{65}^{-2}$ M$_\odot$ yr^{-1} range. No objects with much higher mass formation rates are seen. At lower redshifts the upper envelope falls rapidly. For q_0=0.5 we have used $H_0 = 50$ km sec^{-1} Mpc^{-1} (Fig. 2b) to provide an acceptable age for the universe. With this smaller Hubble constant the maximum luminosities and mass formation rates are similar to those in the q_0=0.02 case.

The distribution of $\dot{M}$ in various redshift bins, computed using the $1/V$ method, is shown for open and flat geometries in Figure 3. The star formation rate may be directly compared with the local star formation rate determined by Gallego et al. (1995) from their Hα survey, which covered redshifts $z \lesssim 0.045$, for a 470 deg^2 sample with EW(Hα+[N II])$>$ 10Å. This is shown for $z = 0.1 - 0.4$ in the bottom right panel of Figure 3. The data points lie roughly a factor of two higher than the Gallego et al. points, although both data sets are fully consistent in slope within the respective 2σ errors and uncertainties. Interestingly, this same difference betwen the number density of local vs. distant galaxies is seen in the K-band count analysis of Huang et al. (1997), who suggested that there is a local deficiency of galaxies by a factor of 2 on scale sizes out to $\sim 300\ h^{-1}$ Mpc. Applying such a factor of 2 correction to the local SFR normalization would then directly match the data at $z = 0.1 - 0.4$.

There is a significant evolution in the maximum mass formation rates with redshift for both open and flat geometries, in the sense that galaxies with much higher formation rates are seen at the higher redshifts (e.g., Cowie et al. 1996). For $z = 0.8 - 1.6$ there are 27 galaxies with $\dot{M} > 10$ M$_\odot$ yr^{-1} while none are seen at $z < 0.8$. Even allowing for the relative volumes the probability of their being drawn from the same distribution function is only 6×10^{-3} for q_0=0.02 and 3×10^{-3} for q_0=0.5. However, the volume density of the rapid star formers is not high. For q_0=0.02 the volume density of objects with $\dot{M} > 10\, h_{65}^{-2}$ M$_\odot$ yr^{-1} is $5.4 \times 10^{-4}\, h_{65}^{-3}$ Mpc^{-3} at $z = 0.8 - 1.6$ and $1.0 \times 10^{-4}\, h_{65}^{-3}$ Mpc^{-3} for $z = 1.6 - 3.2$, while for q_0=0.5 and $\dot{M} > 10\, h_{50}^{-2}$ M$_\odot$ yr^{-1} the densities are $6.2 \times 10^{-4}\, h_{50}^{-3}$ Mpc^{-3} at $z = 0.8 - 1.6$ and $2.2 \times 10^{-4}\, h_{50}^{-3}$ Mpc^{-3} for $z = 1.6 - 3.2$.

4. Discussion

In order to connect these results to the present epoch we need the mass distribution and universal mass density of the local galaxy sample, and these are best derived from the K-band observations. There is still some disagreement in the derived values of the local K-band luminosity function, and we adopt here the average of the samples of Mobasher, Sharples,

& Ellis (1993), Glazebrook et al. (1995b), and Cowie et al. (1996), which corresponds to a Schechter function $M_{K*} = -24.2$ ($+5\log_{10}\ h_{65}$), $\alpha = -1.1$, and $\phi_* = 2\times10^{-3}\,h_{65}^3$ Mpc^{-3}. The disagreement in M_{K*} is ~ 0.5 mags. Most of the light density of the universe is contained in objects near L_*, with 50% of the light density in objects brighter than $\langle L\rangle = 0.7L_*$. Most of these brighter galaxies are earlier than Sb based on their B, I, K colors (Huang et al. 1997), and for consistency we have converted from K magnitudes to masses using the Bruzual & Charlot (1996) models, with $F_\nu = 2.5\times10^{29}$ ergs s^{-1} Hz^{-1} at 21000 Å corresponding to a stellar mass of 10^{11} M$_\odot$, whence L_* corresponds to $1.4\times10^{11}\ h_{65}^{-2}$ M$_\odot$. The local stellar mass density of the universe is then $2.8\times10^8\ h_{65}^{-2}$ M$_\odot$ Mpc^{-3}.

The present-day spectra of the spiral galaxies are well represented by evolutionary models with exponentially decaying star formation rates. Bruzual & Charlot (1993) fit an Sb galaxy with a $\tau_{SFR} = 2$ Gyr and an age of 8 Gyr, and an Sc galaxy with a $\tau_{SFR} = 7$ Gyr and an age of 12 Gyr. In Figure 2 we show the predicted luminosities for such exponentially evolving galaxies, with masses corresponding to L_* for $\tau_{SFR} = 1$ Gyr and $\tau_{SFR} = 2$ Gyr, and to 0.5 L_* for $\tau_{SFR} = 7$ Gyr, for comparison with the observed luminosities. Because both L_* and the observed galaxy luminosities scale as h^{-2}, the curves can only be adjusted via the x-axis conversion from redshift to time and by the choice of the geometry, so the absolute agreement in the normalization of observed and predicted luminosities with redshift shows impressive consistency. For q_0=0.02 we can fit the envelope with an H$_0$ = 65 km sec^{-1} Mpc^{-1} and a late formation epoch $z_f = 3$ model, but for q_0=0.5 we need a low Hubble constant (H$_0\lesssim$50 km sec^{-1} Mpc^{-1}) and an early formation epoch ($z_f \sim 10$). Basically, to match the fall of the maximum luminosity with redshift at $z < 1$, we require galaxy ages of very roughly 4 Gyr at $z = 1$. The expected luminosity envelope is better matched for the $q_0 = 0.02$ case, while for q_0=0.5 there are fewer high luminosity galaxies at high redshift to form the more massive spiral galaxies. Later type galaxies, such as the 0.5 L_* Sc shown by the dotted line in Figure 2, are also consistent with the observations provided they are not too massive, so that their luminosities are not too high at the lower redshifts. A requirement of the models is therefore that the later type galaxies should have lower K luminosities than the earlier types, with Scs being at least a magnitude fainter than Sbs, and Sds being considerably fainter still. The current K-band data are not yet adequate to robustly investigate type dependence in the luminosity function, but this prediction should shortly be testable.

We can now quantify the problem with the q_0=0.5 geometry: Predicted luminosities of the early stages of near-L_* spirals are well above the detection limit (Fig. 2b), at least for galaxies earlier than Sb, and these galaxies must have formed early ($z_f \gg 3$) to provide large enough ages for their ultraviolet luminosities to match the observed redshift evolution and falloff at $z \sim 1$. Thus, in this case we should see a number density of galaxies in the $z = 1.75 \rightarrow 3$ range which is comparable to the present-day number density ($2.2\times10^{-3}\ h_{65}^3$

Mpc^{-3} for $L > 0.25\ L_*$ and $1.1 \times 10^{-3}\ h_{65}^3$ Mpc^{-3} for $L > 0.5\ L_*$). Even if all the unidentified objects are allocated to this redshift range there are only 10 objects, corresponding to a number density of $4.3 \times 10^{-4} \pm 1.5 \times 10^{-4}\ h_{65}^3$ Mpc^{-3}. For q_0=0.02 the number densities are similar, but the problem can be avoided because the formation can begin in this redshift range, so that number conservation is not required. In this case only a fraction of the disks can have begun to form at $z > 2$ with the remainder starting up at lower redshifts.

In any given redshift interval we can compute the total universal mass density formation rate, $\dot{\rho}$, in observed objects, which corresponds to a lower limit on $\dot{\rho}$. Correcting for the incompleteness is not straightforward since it depends on the present-day type mix as a function of mass and the age at a given redshift. However, including only the observed objects and without correcting for faint end incompleteness, we find mass formation rates of $\dot{M} = (1.4 \times 10^{-2}, 1.7 \times 10^{-2}, 1.0 \times 10^{-2}, 2.8 \times 10^{-3})\ h_{65}^{-2}$ M$_\odot$ Mpc^{-3} yr^{-1} for z = (0.2, 0.6, 1.2, 2.4) and q_0=0.02, though these numbers are not directly comparable because of the varying cutoff in $\dot{M}$ so that formation rates at high redshift are relatively underestimated. For objects with $\dot{M} > 10$ M$_\odot$ yr^{-1}, where all objects would be detected at all of these redshifts, the average formation rates are $(0.0, 0.0, 7.1 \times 10^{-3}, 2.8 \times 10^{-3})\ h_{65}^{-2}$ M$_\odot$ Mpc^{-3} yr^{-1}. The overall rates are sufficient to form the present-day mass, so that the open models do appear to provide a fully self-consistent description with the formation peaking at $z \sim 1$ at least for the objects with higher star formation rates.

5. Conclusion

We conclude that in a q_0=0.02 universe we can understand much of the recent history of galaxy formation in terms of the pure luminosity evolution of various spiral galaxy types, provided only that Sc galaxies are at least a magnitude fainter in K than the average of galaxies earlier than Sb, with Sds yet fainter. Models with q_0=0.5 predict too many bright objects at higher redshifts. The conclusion that this works well for q_0=0.02 geometries but not for flat geometries is intimately connected with pure luminosity evolution modelling of the number counts and redshift distributions (e.g., Metcalfe et al. 1996), where q_0=0.5 models tend to produce elbows in the counts and fail to reproduce the faint-end counts. The reason for this is that in the flat models the early stages of the spirals have near-constant and relatively bright magnitudes at all high redshifts (Cowie 1988) — the same problem we encounter here with a radically different approach. The q_0=0.02 models do not suffer from this problem and have much more latitude in available time and volume to resolve the high number count problem (Lilly, Cowie, & Gardner 1991), and also do achieve broad consistency

(Metcalfe et al. 1996) with optical and IR number counts and redshift distributions in this geometry.

The authors are extremely grateful to Stéphane Charlot for comments and help with the Bruzual-Charlot models, to Richard Ellis for providing the Autofib data, and to Josh Barnes Arif Babul, Harry Ferguson, and Mike Fall for useful comments on an earlier draft. This work was supported by the State of Hawaii and STScI grant GO-5922.01-94A.

REFERENCES

Broadhurst, T. J., Ellis, R. S., & Shanks, T. 1988, MNRAS, 235, 827

Bruzual A., G., & Charlot, S. 1993, ApJ, 405, 538

Bruzual A., G., & Charlot, S. 1996, in preparation

Colless, M. M., Ellis, R. S., Taylor, K., & Hook, R. N. 1990, MNRAS, 244, 408

Cowie, L. L. 1988, in The Post-Recombination Universe, ed. N. Kaiser & A. Lazenby (Dordrecht: Kluwer), 1

Cowie, L. L., Hu, E. M., & Songaila, A. 1995, Nature, 377, 603 [astro-ph/9510045]

Cowie, L. L., Songaila, A., & Hu, E. M. 1991, Nature, 354, 460

Cowie, L. L., Songaila, A., Hu, E. M., & Cohen, J. G. 1996, AJ, 112, 839 [astro-ph/9606079]

Ellis, R. S., Colless, M., Broadhurst, T., Heyl, J., & Glazebrook, K. 1996, MNRAS, 280, 235 [astro-ph/9512057]

Gallagher, J. S., Bushouse, H., & Hunter, D. A. 1989, AJ, 97, 700

Gallego, J., Zamorano, J., Aragón-Salamanca, A., & Rego, M. 1995, ApJ, 455, L1

Glazebrook, K., Ellis, R. S., Colless, M. M., Broadhurst, T. J., Allington-Smith, J. R., & Tanvir, N. R. 1995a, MNRAS, 273, 157 [astro-ph/9503116]

Glazebrook, K., Peacock, J. A., Miller, L., & Collins, C. A., 1995b, MNRAS, 266, 65 [astro-ph/9502094]

Huang, J.-S., Cowie, L. L., Gardner, J. P., Hu, E. M., Songaila, A., & Wainscoat, R. J. 1997, ApJ, 476, 12 [astro-ph/9610084]

Kennicutt, R. C., Jr. 1992, ApJ, 388, 310

Lilly, S. J., Cowie, L. L., & Gardner, J. P. 1991, ApJ, 369, 79

Lilly, S. J., LeFèvre, O., Hammer, F., & Crampton, D. 1996, ApJ, 460, L1 [astro-ph/9601050]

Lowenthal, J. D. et al. 1997, ApJ, in press [astro-ph/9701244]

Madau, P., Ferguson, H. C., Dickinson, M. E., Giavalisco, M., Steidel, C. C., & Fruchter, A. 1996, MNRAS, 283, 1388 [astro-ph/9607172]

Metcalfe, N., Shanks, T., Campos, A., Fong, R., & Gardner, J. P. 1996, Nature, 383, 236

Mobasher, B., Sharples, R. M., & Ellis, R. S. 1993, MNRAS, 263, 560

Seaton, M. J. 1979, MNRAS, 187, 73P

Songaila, A., Cowie, L. L., Hu, E. M., & Gardner, J. P. 1994, ApJS, 94, 461

Songaila, A., Cowie, L. L., & Lilly, S. J. 1990, ApJ, 348, 371

Steidel, C. C., Giavalisco, M., Pettini, M., Dickinson, M., & Adelberger, K. L. 1996a, ApJ, 462, L17 [astro-ph/9602024]

Steidel, C. C., Giavalisco, M., Dickinson, M., & Adelberger, K. L. 1996b, AJ, 112, 352 [astro-ph/9604140]

Toth, G., & Ostriker, J. P. 1992, ApJ, 389, 5

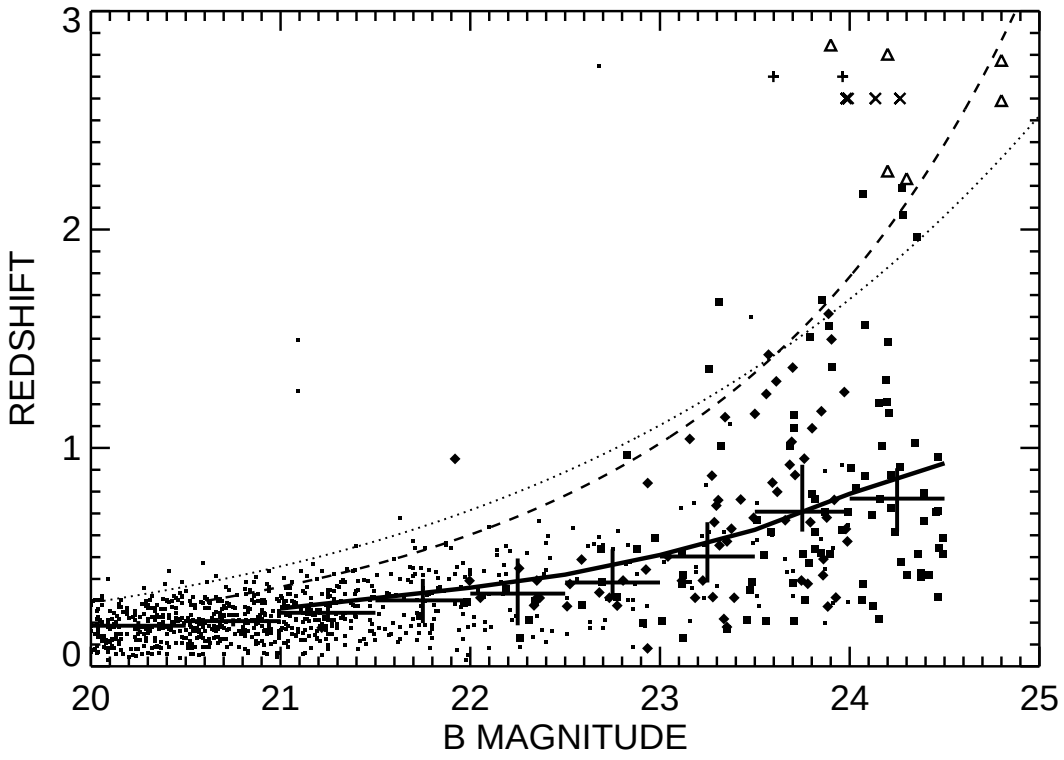

Fig. 1.— The redshift-B magnitude distribution for SSA22 $B < 24.5$ (solid boxes) and SSA13 $B < 24$ (diamonds). Unidentified objects are shown as crosses at nominal redshifts of $z = 2.6$ (SSA22) and $z = 2.7$ (SSA13). The very small symbols show the large Autofib sample of Ellis et al. (1996). The few points lying outside of the well-populated regions are AGN. The large crosses show the median redshifts computed in half-magnitude intervals with $\pm 1\sigma$ error bars computed using the median sign method. (The Autofib data are included at $B < 23$ only.) These are very well described by the no-luminosity-evolution model of Glazebrook et al. (1995a) (solid line). The dashed (q_0=0.5) and dotted (q_0=0.02) lines show the B-magnitude vs. redshift relation for a flat F_ν galaxy which roughly matches the upper envelope of the observed objects in the $z = 1 - 2$ range. We also show (open triangles) the six $B < 25$, $z > 1.6$ galaxies which have been identified in the Hubble Deep Field to date (Cohen et al. 1996; Steidel et al. 1996b; Lowenthal et al. 1997). This rather heterogeneously selected sample shows rough consistency with the upper envelope of the $B - z$ relation seen in the magnitude-selected sample, as do other galaxies selected with the ultraviolet break color techniques (Steidel et al. 1996a), though they may also contain a small number of more luminous galaxies.

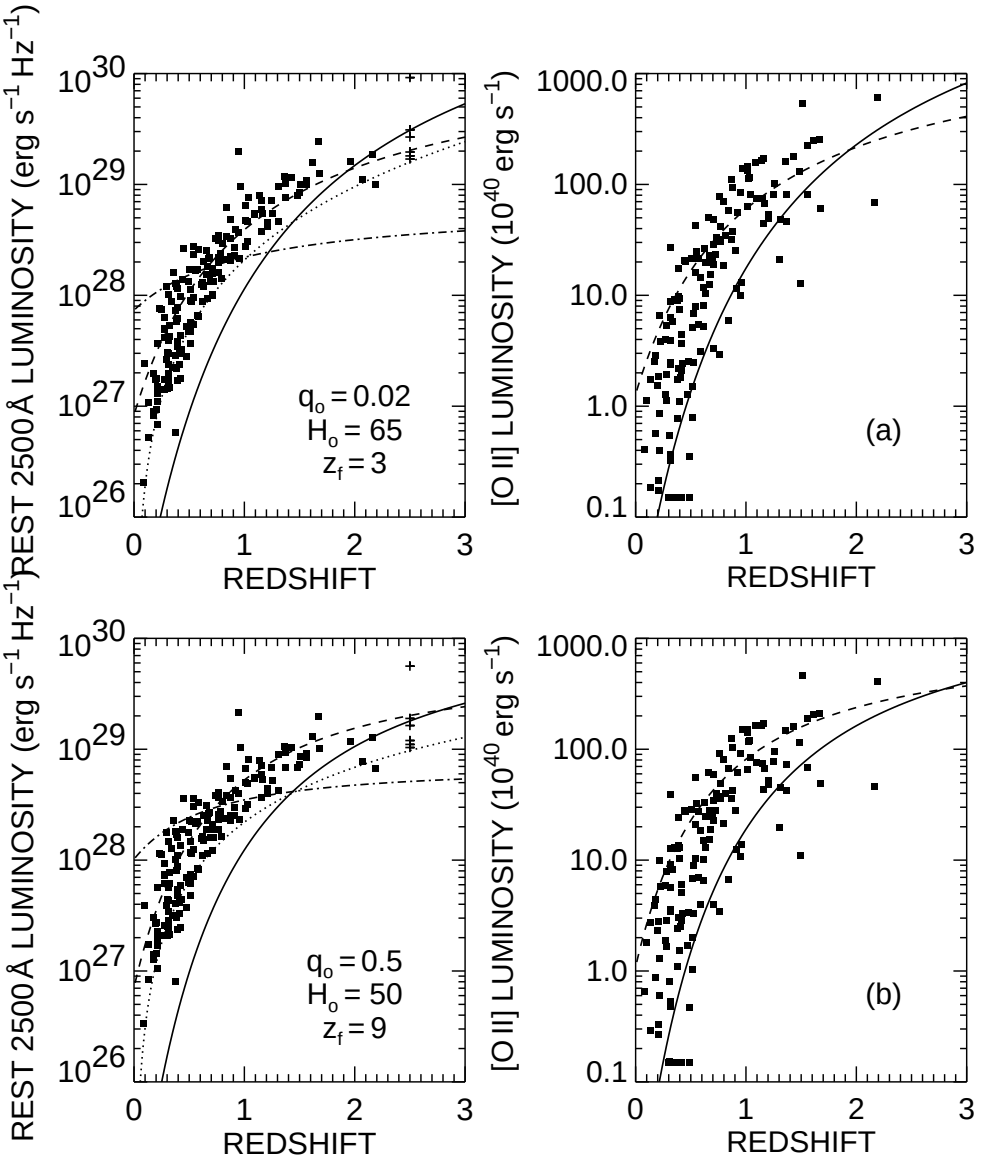

Fig. 2.— The rest frame 2500 Å luminosity (left panels) and [O II] luminosity (right panels) computed for two geometries — q_0=0.02 and $H_0 = 65$ km sec^{-1} Mpc^{-1} (a) and q_0=0.5 and $H_0 = 50$ km sec^{-1} Mpc^{-1} (b). In the left-hand panels the dotted line shows the selection limit for a $B = 24.5$ galaxy with a flat F_ν spectrum. Unidentified objects are shown as crosses at a nominal redshift of 2.5. Models are shown for exponentially decaying star formation rates which would form a $1.4 \times 10^{11}\ h_{65}^{-2}$ $M_\odot$ galaxy with $\tau = 1$ Gyr (solid line), and $\tau = 2$ Gyr (dashed line), or a $7 \times 10^{10}\ h_{65}^{-2}$ $M_\odot$ galaxy with $\tau = 7$ Gyr (dash-dot line). For the open geometry the galaxy evolution is started at $z_f = 3$ and for the flat geometry at $z_f = 9$.

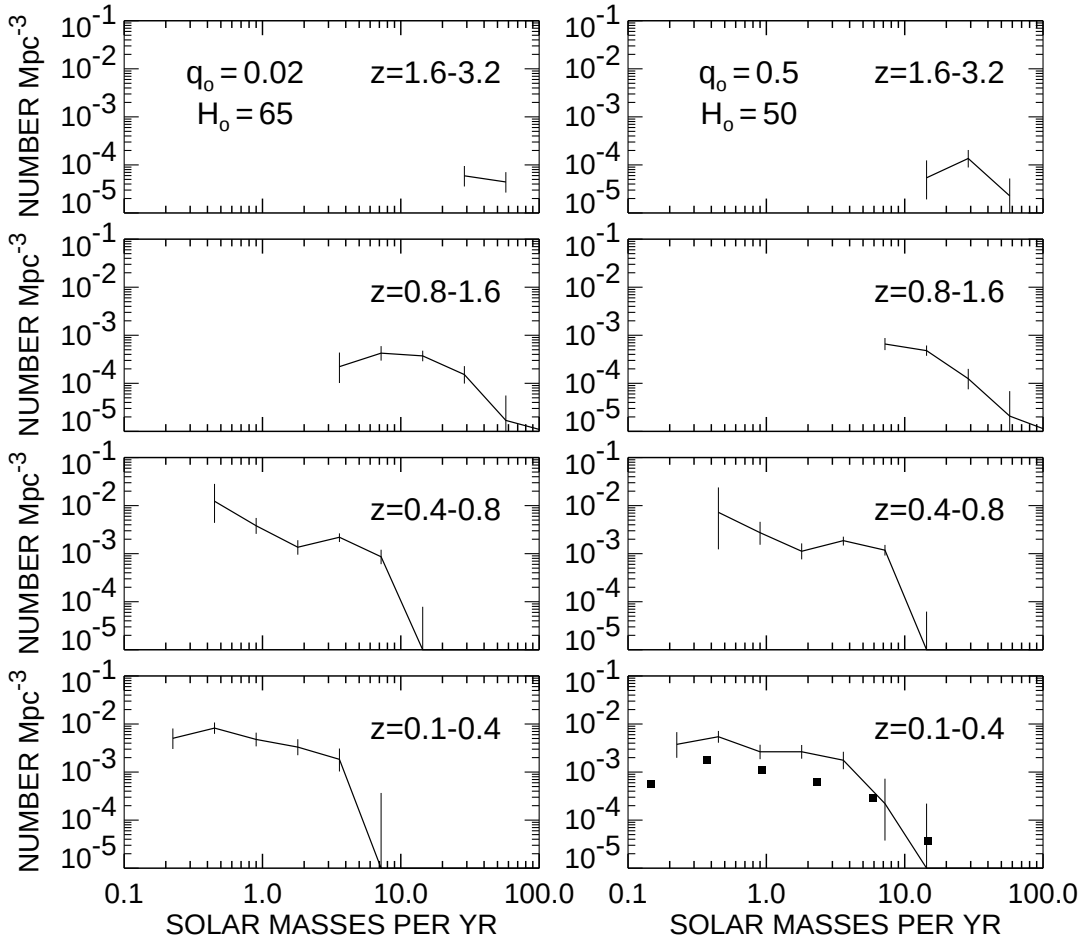

Fig. 3.— The distribution function of the star formation rates as a function of redshift interval for q_0=0.02 (left panels) and q_0=0.5 (right panels). The vertical axis shows the number of galaxies per Mpc^3 per logarythmic bins of 0.3. The errors are $\pm 1\sigma$ based on the number of objects in each bin. The filled squares show the local ($z \lesssim 0.045$) SFR of Gallego et al. (1995), plotted for the Salpeter IMF assumed for the present calculations. (The Hα luminosity corresponding to a star formation rate of 1 solar mass per year is a factor of 3 times higher than for the Scalo IMF, less rich in massive stars, used in the Gallego et al. paper.) Error bars ($\pm 1\sigma$) for these points, based on the number of objects per bin, are comparable to the symbol size; for the endmost points, they are roughly twice the symbol size. The agreement in shape between these two curves is good, with the SFR for the $z = 0.1 - 0.4$ range approximately a factor of two higher than for the Gallego et al. sample. Differences between the two curves are likely to arise due to differences in each sample's completeness in identifying star-forming galaxies, as well as a possible deficiency in local galaxies (Huang et al. 1997).